Vibrational Raman spectra of N_2 in the critical region

M. J. Clouter, H. Kiefte, and C. G. Deacon
Department of Physics, Memorial University of Newfoundland, St. John's, Newfoundland, Canada A1B 3X7
(Received 16 May 1985)

Line-shape data have been obtained for the polarized Raman (Q branch) spectrum of N_2 in the critical region. The high-resolution data were recorded under isochoric conditions at densities ranging from 0.6 to 2 times the critical density (ρ_c) and at reduced temperatures [$\epsilon=(T-T_c)/T_c$] in the range from 8×10^{-5} to 7×10^{-2}. The spectra are shown to be inhomogeneously broadened for $\epsilon<10^{-3}$ on the critical isochore. This is consistent with the presence of long-lived spatial fluctuations in the molecular environment which can be described in terms of a probability distribution for local density. The results are shown to be consistent with a Gaussian distribution whose full width at half maximum exhibits an exponential approach to a maximum value of $\sim0.5\rho_c$ at the critical point.

I. INTRODUCTION

The experimental investigation of anomalous behavior in the vibrational Raman spectra of near-critical fluids has been reported in a number of publications[1-4] from this laboratory. The most recent of these[4] briefly outlines a method of data analysis which confirms that, while the (normal) spectrum of N_2 is homogeneously broadened for $\epsilon>10^{-3}$, it undergoes a continuous change to an inhomogeneously broadened form as $\epsilon\rightarrow0$ along the critical isochore. Theoretical predictions of this effect had previously appeared in the literature,[5,6] but it was not clear whether the ϵ values involved would be sufficiently large to permit experimental observation. Not only has this question now been resolved, but the results[4] are of more far-reaching importance because they constitute the first experimental probe of the probability distribution for local density, i.e., $P(\rho)$, within a near-critical fluid.

The purpose of the present paper is to introduce additional experimental data and to provide details of the analysis procedures which are not included in the necessarily brief publication referred to above.[4] First, however, we present a brief survey of relevant background information.

The Raman spectrum corresponding to a given mode of molecular vibration[7] normally consists of three distinguishable branches designated according to convention as O, Q, and S. The depolarized S and O branches arise respectively from sum and difference transitions involving both the rotational and vibrational degrees of freedom, while the highly polarized Q branch is appropriately referred to as the pure vibrational component. Typically, the spectral widths of the former are orders of magnitude greater than the latter, which in many cases can only be properly resolved via interferometric, or more sophisticated, techniques. In this paper we are concerned exclusively with the behavior of the pure vibrational, or Q-branch, component.

It has long been known that the pure vibrational Raman spectrum for a noncritical fluid depends in an important way upon the density and temperature. The associated literature is quite extensive and the reader is referred to a recent review cited under Ref. 8. The early investigations were concerned primarily with understanding the variations in Raman shift as observed in the gas phase, and with extracting information pertaining to the intermolecular interactions. The theoretical approach[9] recognized that a given molecule was subject to the influence of a fluctuating external field due to its neighbors, and that the anharmonicity of a particular vibrational mode would give rise to a corresponding effect upon the resonant frequency. Since this effect was reflected in the experimental measurements only as an average over space and time, it was necessary to think in terms of a *mean field* which was conveniently defined[10] by a spatial average over all molecules in a frozen configuration. The variation in Raman shift was then expressible in terms of the pair correlation function, and ultimately as a power series in the density with temperature-dependent coefficients.

This treatment was quite successful in accounting for the observed isothermal behavior for H_2 which typically involved a linear (density) dependence of the shift at low densities, and a nonlinear behavior at near-liquid densities. The observed temperature dependence was also readily understood with respect to the relative importance of the repulsive versus attractive parts of the intermolecular potential: the expected repulsive character of the mean field at high temperatures was reflected as a positive slope in the density dependence, while the predominance of attractive forces at low temperatures resulted in a negative slope.

As long as it is understood that only the Raman *shifts* are being considered, these ideas are also applicable to the totally symmetric modes[10] of molecular species other than H_2, but some caution should be exercised in noting that, strictly speaking, the theoretical predictions refer to the *center of gravity* (or alternatively the *band origin*) of the observed spectrum. In the usual case of symmetric spectra this poses no problem, and measurements of the peak position are quite appropriate. However, there are circumstances where the unresolved Q-branch spectrum is characterized by an asymmetry which is itself density

dependent, and the result is a nonlinear density dependence of the peak position. Examples of this have been observed in the low-density spectra[3] of N_2, O_2, and CO, but equally important are the observations of extended linear regions (for CH_4 and CF_4 as well) which are consistent with the above theory.

In the context of this theory, the quantity which is referred to simply as the *density* should properly be regarded as the *local density* within a spherical volume element whose radius is determined by the range of the intermolecular (pair) potential. The definition of this range is somewhat arbitrary but, taking the Lennard-Jones potential as an example, it is apparent that a radius of three times that corresponding to the potential minimum will encompass the most important part of the interaction. For N_2 this yields a value of approximately 1 nm which is typical for the simplest nonpolar molecules.[11] It is of course, clear, both from basic theory and experiment, that normal (noncritical) fluctuations in this local density ρ are not detectable, and are unlikely to have any observable effect upon the spectrum in question. Under near-critical conditions, however, this may no longer be the case, and inhomogeneous broadening could be significant if other possible contributions to the width remain appropriately small.

An assessment of the problem of competing line-broadening mechanisms leads necessarily to a consideration of dynamical effects which play no role in the theory of the Raman shift. This topic has been reviewed in detail by others,[6] and has been briefly surveyed in a previous publication[3] from this laboratory. As emphasized in Ref. 4, the first requirement of the system is that energy relaxation (i.e., T_1) processes not play a major role in determining the width of the noncritical spectrum. Such processes are not significantly influenced by the low-frequency (hydrodynamic) fluctuations in the molecular environment which constitute the critical phenomenon, and are consequently not expected to exhibit any anomalous behavior. T_1 broadening could therefore act simply as a mask of critical effects which might otherwise be observable. The remaining line-broadening mechanisms can be grouped under the heading of *adiabatic vibrational dephasing* (i.e., T_2) processes, or simply *dephasing* processes if it is understood that energy relaxation is excluded from consideration. These include three identifiable effects which can be described as follows: (i) dephasing via resonant transfer of vibrational excitations between molecules, (ii) indirect dephasing via the rotational degrees of freedom and the vibration-rotation interaction, and (iii) so-called *pure* dephasing via direct perturbation of the vibrational motion. The relative importance of these effects for a number of molecular systems has been assessed in a previous publication.[3] It was concluded that (ii) and (iii) above were of importance for N_2, while for CH_4 only (iii) was operative (with a possible secondary contribution from energy relaxation processes). N_2 was chosen for investigation in the present work because it exhibited the largest known critical effect, and also because experimental data for both the shift and width as a function of (noncritical bulk) density, $\bar{\rho}$ had already been obtained.[3,12]

While dephasing processes are in principle operative at all frequencies, it has become clear that the normal liquid is characterized by a Lorentzian spectrum for which the so-called *fast-motion* regime is appropriate. In this regime it is required[5,6] that $\Gamma\tau_c \ll 1$, where τ_c is the correlation time for density fluctuations within the fluid, and Γ is the mean amplitude of variation in vibrational frequency arising from these fluctuations. The opposite extreme of *slow motion* ($\Gamma\tau_c \gg 1$) is of special importance for the particular case of hydrodynamic fluctuations because a large increase in the associated τ_c is known to occur as the critical point is approached. Consequently, if this correlation time becomes sufficiently large within the accessible range of ϵ values (i.e., $\epsilon > 10^{-6}$) one can expect an inhomogeneous contribution to the spectral width of order Γ. However, the observability of this effect is determined by the relative importance of the normally dominant dephasing contribution associated with those modes whose wave vectors k correspond roughly to the first peak in the structure factor $S(k)$. These latter modes are largely unaffected by approach to the critical point, and it is assumed that the associated fast-motion contribution to the linewidth ($\equiv\Gamma_0$) is preserved as in the normal fluid. An approximate criterion for clear detectability of critical broadening is therefore that $\Gamma \gg \Gamma_0$, and Γ_0 can be regarded for convenience as including any T_1 processes which may be of importance.

Γ_0 can in practice be measured on the critical isochore with $\epsilon \simeq 0.1$. Similarly, an upper limit on Γ can be determined from measurements of the normal change in Raman shift which occurs at roughly constant temperature as the density is increased from zero to near the triple-point value. As an example, for the present case of N_2, $\Gamma/\Gamma_0 \simeq 6$ and the critical broadening is easily observable. On the other hand, for $CH_4(\nu_1)$ the corresponding value is $\simeq 2$ and the observed broadening is much less pronounced. These ideas form the basis of the treatment in Ref. 13, where a summary of the available data is also presented.

II. APPARATUS AND EXPERIMENTAL PROCEDURE

The 1-kg sample cell was fabricated from a Be-Cu alloy, and its essential features are shown in Fig. 1. The 0.5 cm^3 internal volume consisted of two mutually perpendicular and intersecting bore holes of 3.2 mm diameter. The four openings involved were closed by quartz windows (W) of 3.2 mm thickness and 10 mm diameter. A fifth access hole at the top of the cell was connected to the external gas-handling system through an isolation valve (V) whose closure point was located about 1 cm above the actual scattering volume. This value was externally activated via a stem of 25 cm length made from thin-walled stainless-steel tubing to provide adequate thermal insulation.

Cooling was accomplished by way of two flexible copper braids (not shown in Fig. 1) which were mechanically clamped to the cell and to the second-stage cold head of a closed-cycle He-gas cryogenerator (Air Products CSA-202). The cell was housed in a vacuum enclosure with an intermediate radiation shield which was thermally

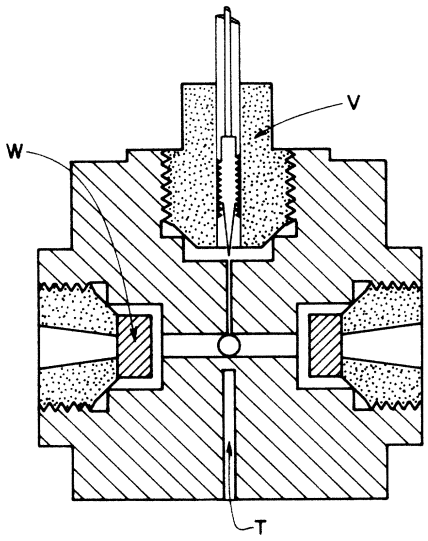

FIG. 1 Be-Cu sample cell. V is the isolation valve, T the Pt thermometer well, and W the quartz windows.

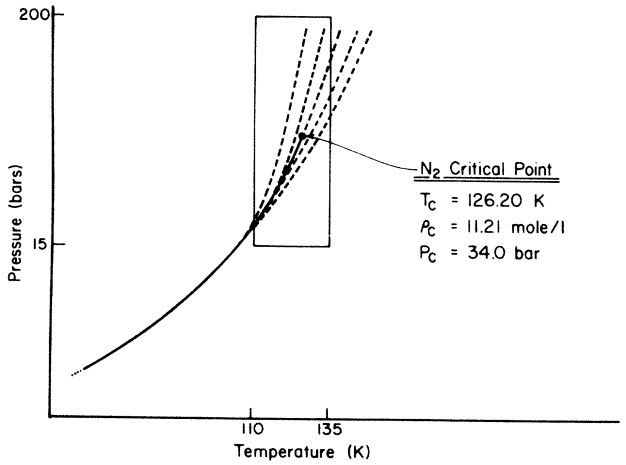

FIG. 2 Schematic representation of the N_2 critical region (rectangular box) in the P-T plane. The solid curve is the liquid-vapor coexistence line, and the dashed curves are representative of the isochoric paths followed in the present experiments. The critical-point data are from Ref. 21.

anchored to the first-stage cooling element of the cryogenerator, and it was maintained at a temperature approximately 50 K above that of the cell. Coarse control of the cooling power was achieved by a feedback control which regulated the temperature of the cryogenerator cold head to within 0.1 K. Fine control was provided by a second feedback loop which included the following elements: (i) a calibrated Pt resistance element (Lakeshore Cryotronics) which was housed in the thermometer well, T, of Fig. 1, (ii) two 25-Ω heaters which were connected in series and mechanically clamped to the body of the cell, (iii) a programmable digital ohmeter (Fluke 8860A), and (iv) a power amplifier. The ohmeter was programmed to compare the resistance of the Pt thermometer (which was usually taken as an average of at least 15 readings) with a preset reference value, and to send an appropriate correction signal to the power amplifier. The latter was capable of delivering a maximum power of about 2 W to the cell heaters which, because of the relatively "soft" thermal contact between the cell and the cryogenerator cold head, was sufficient to maintain a maximum temperature difference of about 10 K between the two. The overall arrangement was characterized by a thermal response time of about 30 s, and provided long-term control which was stable to within 5 mK under optimum conditions.

Experiments were performed only along constant-density (isochoric) paths as shown in Fig. 2, and sample densities were determined with respect to a fixed reference point by using previously determined density versus frequency data for the Q branch peak. The chosen reference point was the saturated liquid at 110 K. The first step in the procedure was to fill the cell with liquid to a level above the closure point of the isolation valve. The temperature was then carefully controlled (at 110 K) while the valve was slowly closed to ensure that the cell was completely filled with liquid under its own vapor pressure. After evacuating the gas lines above the valve, the static pressure in these lines was monitored while the cell temperature was cycled from 110 to 135 K and back to the original temperature. Return of the spectral peak to its initial position was taken as evidence that no sample material had leaked from the cell around the cycle, and this was supported by the constancy of the gas-line vacuum. The spectral peak position at 135 K was thus established as a secondary reference, and subsequent adjustments to sample density were made at this temperature while monitoring the change in the peak position. Although not highly accurate, this method was considered adequate with respect to noncritical densities since spectral broadening was observed over a wide density range. Establishment of the critical density was, however, treated as a special case which required greater accuracy. As previously described,[4,14] this was achieved by visual observation of the liquid-vapor interface in the range $-0.1\ \text{K} < T - T_c < 0\ \text{K}$. The liquid level was first set at the half-height point in the cell, and small adjustments were made until the interface was observed to disappear without vertical movement as the temperature of the isolated sample was slowly raised. This method was very sensitive, and the resultant peak position at 135 K was consistent with that obtained by the less accurate procedure described above.

The cell was designed to accommodate a 90° scattering geometry in the horizontal plane, and the overall arrangement of the apparatus is shown in Fig. 3. The exciting radiation was provided by an Ar^+ laser (Spectra Physics 165-08) operating in a single cavity mode with a nominal wavelength of 514.5 nm and a power output of 150 mW. The scattered radiation was always prefiltered via a narrow-band interference filter (IF) which served to isolate the Raman region of interest for high-resolution study. On occasion, and as described below, the spatial filtering arrangement SF was also employed.

The spectrometer consisted of a scanning Fabry-Perot (FP) interferometer (Burleigh RC-110), a cooled photomultiplier (PMT) detector (ITT FW130), photon-

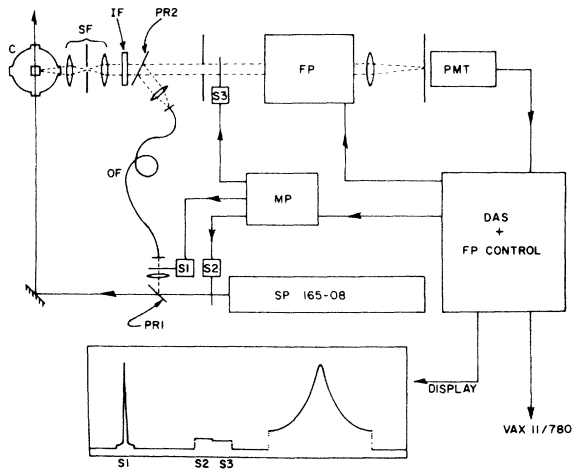

FIG. 3 Schematic diagram of the experimental setup. C is the cryostat; SF the spatial filter; IF the narrow-band interference filter; PR1 and PR2 the uncoated glass reflectors, S1, S2, and S3 the electromechanical shutters, FP the Fabry-Perot interferometer, PMT the cooled photomultiplier tube, OF the optical fiber, MP the microprocessor, DAS the data acquisition system, and SP the Ar^+ laser.

counting electronics, and a combined data-acquisition plus Fabry-Perot control system (Burleigh DAS-1). The spectra were acquired by a process of repetitive scanning with a period of 5 to 10 s, and the total accumulation time required to achieve acceptable signal-to-noise ratio was 12 to 24 h. It was consequently necessary to utilize fully the feedback control capability[15] of the DAS-1 in order to minimize the effects of long term drift in the interferometer alignment. The reference signal required for this purpose would normally be the parasitic Rayleigh peak which was eliminated by filtering in the present case, so that an alternative arrangement was necessary. As shown in Fig. 3, an uncoated glass reflector, PR1, was used to deflect a suitably attenuated sample of the laser output through an optical fiber (OF) when the shutter S1 was open. The light which emerged from the fiber was collimated and accurately directed along the axis of the scattering optics by a second uncoated reflector, PR2, which was positioned downstream from the interference filter IF. The action of shutter S1 was controlled by a microprocessor (MP) which utilized the master clock of the DAS-1 as a time base. S1 was programmed to open at a point nearest the beginning of each sweep where resonant transmission at the laser frequency was about to occur, and it was closed immediately afterward so that no laser radiation reached the detector during scanning of the Raman line. The microprocessor also controlled two other shutters which were used to monitor the PMT dark count (S3) and the ambient background during the "beam-off" condition (S2). Since the dark count was usually within the PMT specifications at about 1 count per second, this provided a convenient means of monitoring the ambient light leakage, and precautions were taken to ensure that the beam-off signal was never more than twice the dark count. Operation of the three shutters required from 10% to 20% of the sweep time. By using the segmented scanning feature of the DAS (which permitted rapid scanning through uninteresting parts of the spectrum) it was consequently possible to devote from 80% to 90% of real experimental time to the accumulation of Raman signal. A representative display, as it would appear on the CRT screen of the DAS, is shown at the bottom of Fig. 3. Data were transmitted from the DAS to a central computer for further processing as described in the next section.

The interferometer was calibrated at the same liquid-N_2 reference point (110 K) mentioned above, by using previous linewidth data[3,12] which were accurate to $\sim 5\%$. The *changes* in linewidth, which are of primary importance in the present work, were consequently considered reliable to at least the same level of accuracy.

We close this section by drawing attention to precautions which were taken to ensure that the observed effects were indeed of a fundamental nature. In the particular case of N_2 it should first be noted that for $\bar{\rho} \approx \rho_c$ the Q-branch width varies approximately as $\bar{\rho}^{-1}$ in the noncritical regime. Spurious broadening associated with a leaking sample cell was therefore always a potential problem. However, a number of routine precautions were taken in this respect. In particular, the temperature of the sample was returned to its original value at the conclusion of each series of isochoric measurements which usually involved several days. If the initial position of the spectral peak was not accurately recovered, the entire series of measurements was discarded. Among the very few other extraneous mechanisms which could conceivably influence the spectral distribution of Raman intensity, the most likely possibility was considered to be a combination of gravitation and multiple scattering. The former is known to give rise to vertical density gradients in a near-critical fluid, and problems could result if multiple scattering from different vertical levels in the sample were significant. However, such an effect was considered negligible on the basis of two observations. First, the downward deflection of the transmitted laser beam which would result from refraction through such a density gradient was not present when line-broadening observations were made. Second, while multiple Rayleigh scattering was obviously significant (at the lowest ϵ values on the critical isochore), corresponding effects on the Raman spectrum were assessed by using a spatial filter (SF in Fig. 3) and were found to be negligible. The size of the circular restricting aperture was in fact varied from a 500 μm diameter down to 50 μm without any observable effect on the spectral distribution of the Raman intensity, even under the most severe conditions of multiple Rayleigh scattering. This finding is of course consistent with the main body of linewidth data which shows that critical broadening persists at $(\bar{\rho},\epsilon)$ values which are well outside the range associated with gravitational and multiple-scattering effects.

III. RESULTS

Six different densities $\bar{\rho}$ were used in the range from $0.6\rho_c$ to $2\rho_c$, and in each case the $T-T_c$ value was varied from 0.01 K ($T=126.21$ K, $\epsilon=8\times10^{-5}$) to 8.8 K

($T=135$ K, $\epsilon=7\times10^{-2}$) in a maximum of eight steps. The largest spectral broadening effect was observed in the data for $\bar{\rho}=\rho_c$ which have already been published.[4] In the present paper we present data for the case $\bar{\rho}=1.2\rho_c$, which displays the largest asymmetry, as well as for the extremes of density quoted above, which clearly indicate the wide scope of the anomalous behavior.

The 512-channel output from the DAS was processed on a Digital Equipment Corporation VAX 11/780 computer. The first stage involved three steps which are briefly described as follows. (i) An average background level was calculated from the 10- to 20-channel signal provided by shutter S2. This value was stored for later use, together with other manually entered parameters such as free spectral range, temperature, pressure, etc. (ii) The data for the instrument function, as provided by shutter S1, was processed by a least-squares routine which yielded a two-parameter fit to the theoretically predicted Airy function.[16] The latter is given by $S_I(\nu)=C_1/[1+C_2\sin^2(\pi\nu/R)]$, where C_1 and C_2 are the adjustable parameters which determine peak height and width, respectively, R is the known free spectral range of the interferometer, and ν is the frequency relative to the peak of the profile. Although other more elaborate functions provided better fits, use of the Airy function was found not to compromise the accuracy of the overall analysis since the widths involved were rarely more than 10% of the Raman width, and subsequent deconvolution procedures constituted only a minor correction to each spectrum. (iii) Most of the original DAS output was now discarded; only the approximately 200 points comprising the Raman spectrum were retained with appropriate channel identifiers for recovering the position of the spectrum relative to the peak of the laser reference line.

The second stage of the data processing was devoted to the application of corrections for the finite instrument resolution. In this connection the governing relation is

$$S_O(\nu)=S(\nu)\circ S_I(\nu)\ , \tag{1}$$

where S_O and S represent the observed spectrum and the "true" spectrum, respectively, and $\circ$ signifies the mathematical operation of convolution.[16] As is always the case in spectroscopy, the object is to recover the true spectrum, $S(\nu)$ by a process of *deconvolution,* and this process is nontrivial because the inversion of Eq. (1) cannot be accomplished analytically for functions of arbitrary form. By way of contrast, however, the Fourier transform of Eq. (1) reduces to the simple form[16]

$$\mathcal{F}\{S_O(\nu)\}=\mathcal{F}\{S(\nu)\}\mathcal{F}\{S_I(\nu)\}\ ,$$

or,

$$S'_O(t)=S'(t)S'_I(t)\ . \tag{2}$$

Deconvolution is then achieved by the relatively trivial operation,

$$S'(t)=S'_O(t)/S'_I(t)\ , \tag{3}$$

and $S(\nu)$ is obtained directly as the inverse transform of $S'(t)$. In many cases the Fourier transform operations may be as tedious as the inversion of Eq. (1), so that no advantage is gained. In the present case, however, it is highly advantageous because of the simplicity of the spectra.

The procedure was implemented by employing Fourier series representations for the (periodic) S_I and S_O spectra. Because of the even character of the instrument function, its transform consisted simply of a set of cosine coefficients $A_{I,n}$, which were read directly from the analytical solution[17]

$$A_{I,n}=\left[1+\frac{2}{C_2}[1-(1+C_2)^{1/2}]\right]^n\ , \tag{4}$$

with $n=0,1,2,\ldots$. Numerical calculation of the Fourier coefficients for S_O was normally preceded by three preparatory operations. First, as illustrated in Fig. 4, a standard three-point smoothing routine was applied to the Raman data in order to reduce the undesirable effects of high-frequency noise. Second, an Airy function extrapolation was used to generate the interorder minima which were not normally included in the data and which were required for the transform operation. This procedure was adopted in order to economize on accumulation time, since it was recognized that information pertaining to the wings of the true (i.e., isolated) Raman spectrum was least likely to be recovered with any accuracy from the superimposed wings actually observed. The acceptability of the procedure, which involved only 15 points at each extreme of a given data set, was verified in a number of cases. Third, a smoothing operation was again applied to the spectral wings where high-frequency noise was found to be most troublesome. As distinct from the initial smoothing, this consisted of a selectable n-point ($n<10$) averaging process which was weighted so that its effectiveness was maximum at the extremes of the data while falling rapidly to zero at a point about $0.3R$ from the peak on either side. Consequently, the most important information contained in the central part of the profile was left essentially undisturbed. The S_O profile was in

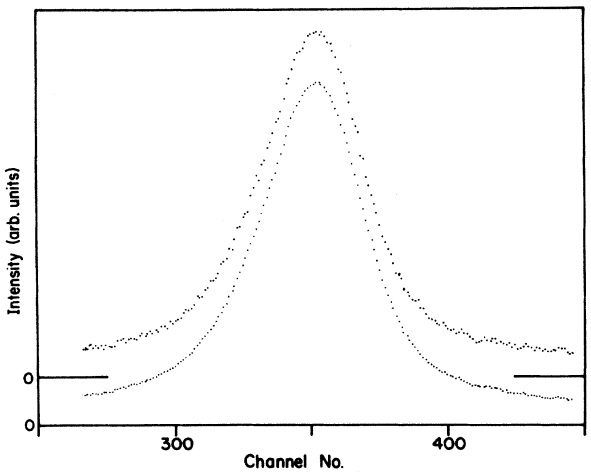

FIG. 4 Unprocessed Raman spectrum (upper profile) as observed on the display screen of the data acquisition system. The lower profile illustrates the effect of numerical low-pass filtering (three-point smoothing).

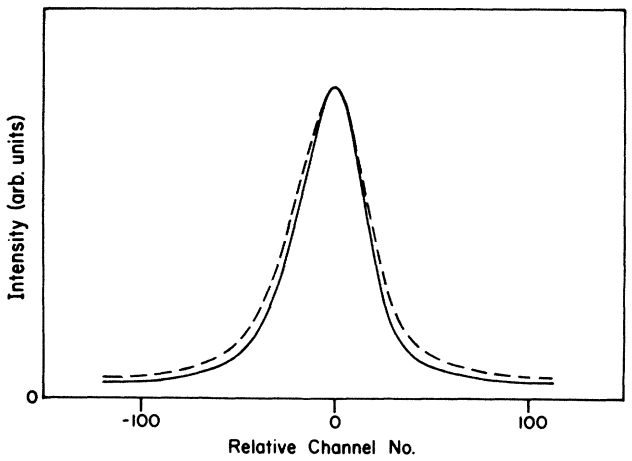

FIG. 5 Comparison of Raman profiles before (— — —) and after (——) correction for instrument resolution.

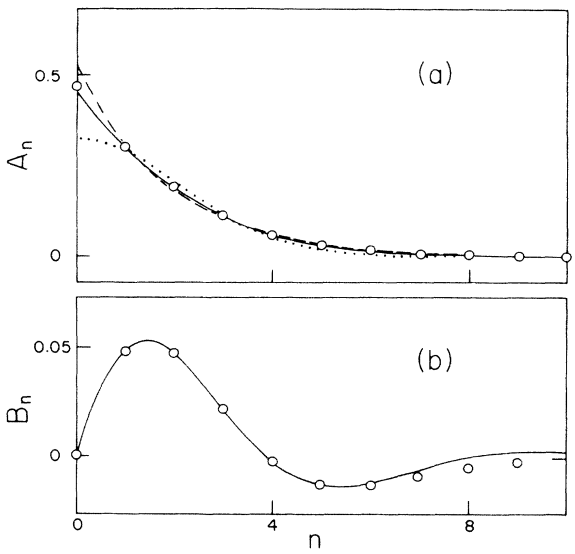

FIG. 6 Fourier series representation (○) of a typical $S(\nu)$ profile; A_n and B_n are the cosine and sine coefficients, respectively. The fitted curves in (a) are identified as follows: Gaussian transform (· · · ·), Lorentzian transform (— — —), Voigt transform (——). For fitted curve in (b) see text.

general asymmetric so that the corresponding Fourier series included both cosine ($A_{O,n}$) and sine ($B_{O,n}$) terms. The number of terms required was determined by a visual comparison (on a video terminal screen) of the inverse transform with the smoothed data. In general it was not possible to distinguish between the two superimposed displays with n in the range $12 \leq n \leq 20$. The deconvolved spectrum S was obtained from a Fourier series with coefficients given, in accordance with Eq. (3), as $A_n = A_{O,n}/A_{I,n}$ and $B_n = B_{O,n}/A_{I,n}$. A comparison of typical profiles for S_O and S is shown in Fig. 5, which also serves to emphasize the relatively minor effect of instrument resolution.

The third stage of the data analysis was concerned primarily with determining the best representation of the $S(\nu)$ spectra in terms of analytic functions. While it was expected that the standard Lorentzian and Gaussian line-shape functions would be of importance in this respect, it was also clear that neither of these functions (nor the hybrid Voigt function) was directly applicable because of the asymmetry which was observed in the near-critical spectra. The approach taken was therefore to investigate independent functional fits to each of the cosine and sine transforms which provided a convenient means of separating the even and odd components of the spectra. The Fourier transforms of the line-shape functions mentioned above were then introduced as the most obvious possibilities for fitting the A_n coefficients; namely,

$$A_L(t) \equiv \mathcal{F}\{L(\nu)\} = \mathcal{F}\{L_0(1+L_1\nu^2)^{-1}\} = l_0 \exp(-l_1 t) , \tag{5}$$

$$A_G(t) \equiv \mathcal{F}\{G(\nu)\} = \mathcal{F}\{G_0 \exp(-G_1\nu^2)\} = g_0 \exp(-g_1 t^2) , \tag{6}$$

$$A_V(t) \equiv \mathcal{F}\{L(\nu) \circ G(\nu)\} = v_0 \exp(-v_1 t - v_2 t^2) . \tag{7}$$

The best fits obtained in a typical case are shown in Fig. 6 where it is clear that the most successful fit is provided by $A_V(t)$. This function was consequently used in the analysis of all the spectra and will subsequently be referred to simply as $A(t) = a_0 \exp(-a_1 t - a_2 t^2)$. A number of different functions were fitted to the B_n coefficients, and the form $B(t) = b_0 \exp(-b_1 t)\sin(b_2 t)$ was chosen as the simplest one which produced acceptable accuracy in the regenerated spectra (see below).

The A_0 coefficient, which was determined by the dc background component in a given spectrum, was not included in the fitting procedure. This discriminated against the presence of any legitimate broadband Raman signal (due to collision-induced scattering, for example) which was not part of the Q branch spectrum and which, strictly speaking, should be excluded from consideration. The price of excluding A_0 was, of course, that the legitimacy of the $A(t)$ function in the region near the origin was open to question, and corresponding inaccuracies could occur in the far wings of the resulting spectra. This possibility was checked by first regenerating an $S(\nu)$ spectrum with A_0 replaced by $A(0)$ in the original set of Fourier coefficients, and then comparing with the inverse transform using coefficients read from the fitted functions $A(t)$ and $B(t)$. The comparison was made after renormalization to the same peak height, and there were no significant differences between the profiles. While this procedure was certainly not infallible, it at least demonstrated that most of the $S(\nu)$ spectrum was reproduced with high fidelity by the fitted transforms.

It should perhaps be emphasized that the procedures described above always lead to $S(\nu)$ spectra with the periodicity required by the Fabry-Perot spectrometer. This characteristic property necessarily results from employing a Fourier series representation where the fundamental frequency is specified (in this case) as R, and the property is entirely independent of the values actually assigned to the Fourier coefficients. In the case of the coef-

ficients given by Eq. (4) there is an *analytic* function $S_I(\nu)$ with the required periodicity, but for $S(\nu)$ it is necessary to think in terms of a superposition of aperiodic functions. For example, the highly symmetric, noncritical spectra are correctly represented by a periodic superposition of Voigt profiles, namely,

$$S(\nu)=\sum_{m=-\infty}^{+\infty} V(\nu+mR)\,, \tag{8}$$

where m is an integer. In the more general case $V(\nu)$ would be replaced by some asymmetric function which we represent simply as $I(\nu)$. In all cases $S(\nu)$ is characterized by the presence of periodic (nonzero) minima which are due to the multiple overlapping of wings so that additional effort is required to extract more complete information pertaining to the $I(\nu)$ profile which is actually of interest. This can, in principle, be accomplished by using the fitted $A(t)$ and $B(t)$ functions for purposes of regular interpolation to increase the total number of Fourier coefficients by some factor, say 5. The $S(\nu)$ spectrum generated by the new set of coefficients then corresponds[16] to

$$S(\nu)=\sum_{m=-\infty}^{+\infty} I(\nu+5mR)\,, \tag{9}$$

i.e., the period is expanded by a factor of 5 so that the interorder overlapping is much less pronounced. In fact, if the minima in $S(\nu)$ are zero to within the noise limits, then the $I(\nu)$ profiles can be regarded as completely separated. Of course, the correctness of this procedure is determined by the details of the $A(t)$ function for $t\rightarrow 0$, where, as previously mentioned, verification is not possible when A_0 is *a priori* undetermined. Nevertheless, the result is certainly a better approximation to the true $I(\nu)$ than $S(\nu)$ itself, and it was on this basis that the procedure was used (with fivefold interpolation) to produce

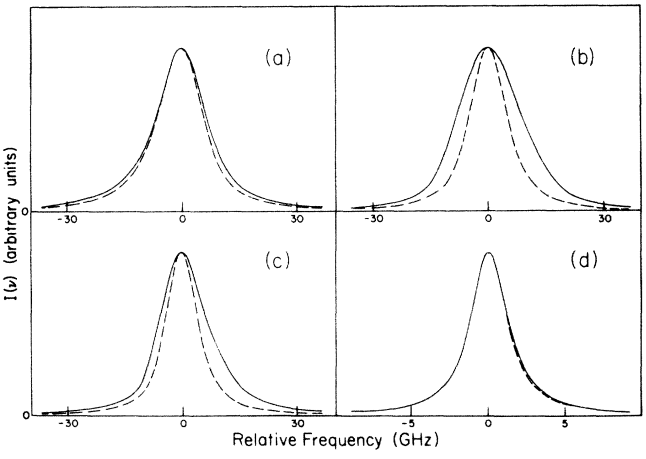

FIG. 7 Final $I(\nu)$ profiles for four different values of $\bar{\rho}$; (a) $0.6\rho_c$, (b) ρ_c, (c) $1.2\rho_c$, and (d) $2\rho_c$. In each case the dashed and solid curves correspond, respectively, to the highest and lowest temperatures investigated. Note that transformation from channel number (Figs. 4 and 5) to frequency involves a left-to-right reversal of the profiles.

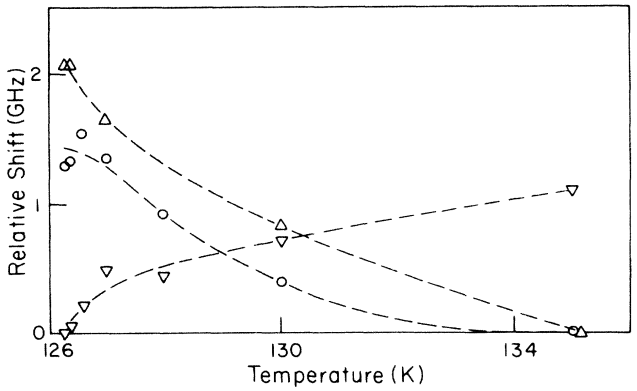

FIG. 8 Temperature dependence of the $I(\nu)$ peak frequency for three different values of $\bar{\rho}$; $\nabla\rightarrow 0.6\rho_c$, $\circ\rightarrow\rho_c$, $\triangle\rightarrow 1.2\rho_c$. Dashed curves are for visual guidance only.

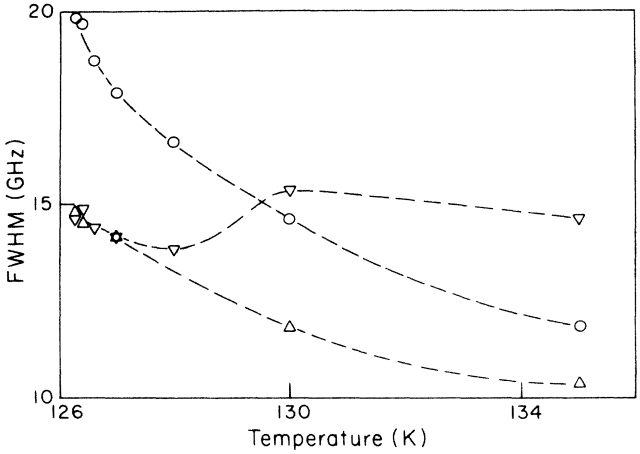

FIG. 9 Temperature dependence of the full width at half maximum for $I(\nu)$ along the three isochores identified in Fig. 8. Dashed curves are for visual guidance only.

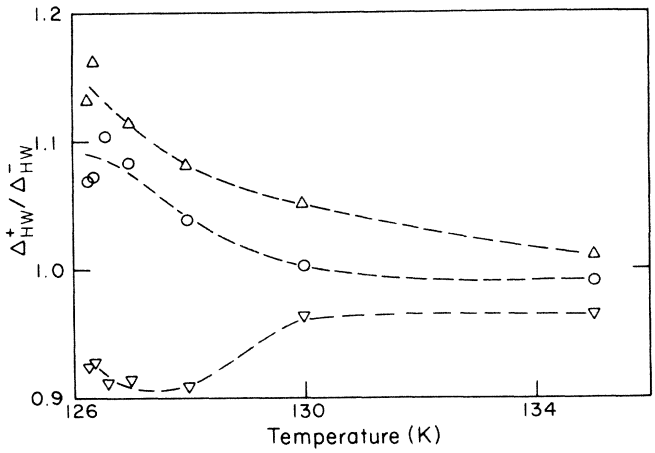

FIG. 10 Temperature dependence of the $I(\nu)$ asymmetry along the three isochores identified in Fig. 8. The asymmetry is measured as a simple ratio of half-widths at half-height, Δ_{HW}: the + and − superscripts identify the $+\nu$ and $-\nu$ sides of each profile, respectively (see Fig. 7). Dashed curves are for visual guidance only.

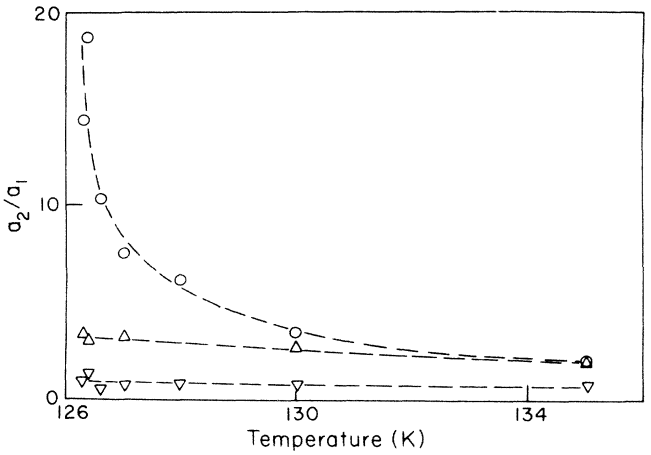

FIG. 11 Relative importance of the Gaussian (a_2) versus Lorentzian (a_1) content of the $I(\nu)$ profiles along the three isochores identified in Fig. 8. Dashed curves are for visual guidance only.

the final profiles whose behavior is summarized in Figs. 7–11. This last step in the data processing should be regarded as somewhat cosmetic, and we again emphasize that any associated inaccuracies in the wings of the profiles have no significant impact on the conclusions of the next section where the information base corresponds to $n \geq 1$ in Fig. 6.

IV. DISCUSSION AND INTERPRETATION

With reference to Fig. 7 it is apparent that (critical) broadening is observed for values of $\bar{\rho}$ within a range whose limits differ by at least a factor of 2, and which is centered approximately at the critical density ρ_c. At the highest density, $\bar{\rho}=2\rho_c$ [Fig. 7(d)], broadening was only marginally detectable for a temperature variation of 25 K which was considerably greater than that employed at the lower densities. The influence of the normal motional narrowing processes[6] is obvious since the width [full width at half maximum (FWHM) of 2.8 GHz] is smaller by roughly a factor of 5 compared to $\bar{\rho}=\rho_c$, and as far as could be determined the profile is pure Lorentzian. In addition, the peak position was found to be independent of temperature to within 0.2 GHz. This demonstrates that the normal, or noncritical, temperature dependence of the spectrum is negligible in the present context, and a possible ambiguity regarding the origins of the lower density behavior is eliminated. The result also has the consequence that spectral broadening previously observed along the liquid-vapor coexistence line[1,3] can now be interpreted as a purely density-dependent effect except, perhaps, in the immediate vicinity of the critical point. In fact, our reexamination of these data clearly indicates a ρ^{-1} dependence in agreement with theoretical prediction.[18]

The minimum experimental density of $0.6\rho_c$ [Fig. 7(a)] does not correspond to a lower bound on the broadening effect. Rather, this case was chosen somewhat arbitrarily to illustrate the complications in spectral behavior which are associated with the emergence of the normal Q-branch shape at the lower densities. This (normal) shape is characterized[18,19] by an asymmetry which is opposite in sense to that associated with the critical broadening observed at higher densities, and this is evident in Fig. 10. The reverse temperature dependence of the peak position (Fig. 8), and the absence of any consistent trend in the width variation (Fig. 9), are also typical of spectra in this density regime.

The spectra for $\bar{\rho}=1.2\rho_c$ [Fig. 7(c)] were included to show that the broadening does not depend strongly on density near ρ_c, so that observation of the effect does not require highly accurate density determinations. The distinguishing feature of these spectra is that they exhibit the largest asymmetry (Fig. 10), but we can offer no explanation as to why this should be.

While attention is naturally drawn to the case $\bar{\rho}=\rho_c$ [Fig. 7(b)] because it exhibits the largest broadening effect (see also Fig. 9), it should also be noted that the temperature dependence of the peak position (Fig. 8) and the asymmetry (Fig. 10) are not similarly distinguished. In fact, as shown in Fig. 11, the most remarkable feature of the spectra recorded on the critical isochore is the development of a pronounced Gaussian character which leads to the interpretation described in the remainder of this section.

Our conclusion based on Fig. 11 is that the slow-motion criterion is satisfied, and that the spectrum is indeed broadened inhomogeneously as the critical point is approached. This, in turn, implies that the near-critical spectrum is actually a superposition of "local" Raman spectra each of which is characterized by (local) values of ρ and T, and is weighted according to the probability of occurrence of these local values. In order to test this hypothesis with available information the following simplifying assumptions were introduced.

(i) The weakness of the T dependence as demonstrated by the data for $\bar{\rho}=2\rho_c$ (above) is assumed sufficient to justify neglecting the effect of temperature fluctuations altogether.

(ii) Each local Raman spectrum is assumed to be identical with that obtained for a bulk noncritical sample at the same density ($\bar{\rho}=\rho$), and roughly comparable temperature.

The local spectrum was consequently chosen initially to be Lorentzian in form [cf. Eq. (5)] with peak frequency (ν_p), FWHM (Δ), and area (intensity) determined entirely by the local density.

In principle then, the synthesis of experimental $I(\nu)$ profiles for $\bar{\rho}=\rho_c$ and $\epsilon\rightarrow 0$ can be achieved by the relation

$$I(\nu)=\int_0^{\rho_m} L(\nu,\rho)d\rho=\int_0^{\rho_m}\rho\mathscr{L}(\nu,\rho)P(\rho)d\rho\ , \quad (10)$$

where $\mathscr{L}(\nu,\rho)$, is a Lorentzian of unit area, i.e.,

$$\mathscr{L}(\nu,\rho)=\frac{2}{\pi\Delta}\left[1+\left[\frac{2\{\nu-\nu_p\}}{\Delta}\right]^2\right]^{-1}\ . \quad (11)$$

A ρ factor occurs in the integrand of Eq. (10) because, as in the normal fluid, the probability of a Raman event is proportional to the (local) density. It guarantees, for ex-

ample, that in the present case $I(\nu)=0$ for the physically plausible case $P(0)>0$. As previously defined, $P(\rho)$ determines the probability for a given ρ and scales the area of $\mathscr{L}$ accordingly. A plausible upper limit on ρ, i.e., ρ_m, is obtained by recognizing that $P(\rho)$ must approach zero for local densities in the neighborhood of the triple-point value [$\rho_{TP}=694$ amagat (Refs. 20 and 21)]. Our initial choice of $\rho_m=4\rho_c=1000$ amagat was found to be acceptable in view of the results obtained. As a first approximation, ν_p was assigned the linear density dependence taken directly from Ref. 3, i.e., $\nu_p=\nu_0-0.09\rho$, where ρ is in amagats and ν_0 corresponds to $\rho=0$.

As previously mentioned, theory[18] predicts a ρ^{-1} dependence for Δ as the motional narrowing limit is approached, and this is supported by data for the saturated liquid. Again as a first approximation, the form $\Delta=a/(1+b\rho)$ was chosen as the simplest variation of the high-density ρ^{-1} behavior which avoids the obvious divergence at low densities. The parameters $a=27$ GHz and $b=0.0055$ GHz amagat^{-1} were chosen to be consistent with the liquid data while approximately reproducing the known value of Δ for $\rho\rightarrow 0$.

The choice of the Gaussian form for $P(\rho)$ is clearly guided by the result of Fig. 11. It is used here in the normalized form

$$P(\rho)=(\sigma\sqrt{2\pi})^{-1}\exp\left[\frac{-(\rho-\bar{\rho})^2}{2\sigma^2}\right], \tag{12}$$

where σ is the square root of the second moment ($=0.425\Delta$), and is the single floating parameter which remains to be determined via Eq. (10).

The practical, computerized realization of Eq. (10) was necessarily limited to the summation of a finite number of $L(\nu)$ profiles. An optimum number of 40 was chosen by noting that an $\sim 20\%$ decrease in this number produced significant changes in the resulting $I(\nu)$ for a given value of σ, whereas a similar increase had no effect. The corresponding ρ values were distributed uniformly over the range from 0 to 1000 amagat so that the interval between ν_p values was 2.25 GHz, and each $L(\nu)$ profile was defined by a series of 200 points. A least-squares routine was used to determine the value of σ which produced the best fit of the synthesized $I(\nu)$ to the experimentally determined $I(\nu)$. The worst-case result of this procedure is shown in Fig. 12, and the corresponding $P(\rho)$ in Fig. 13.

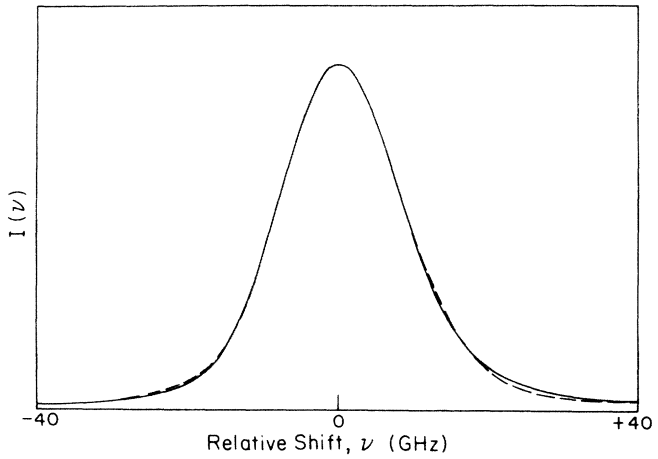

FIG. 12 Comparison of the experimentally determined $I(\nu)$ (——) and the synthesized $I(\nu)$ (— — —) for $\bar{\rho}=\rho_c$ and $\epsilon=8\times10^{-5}$.

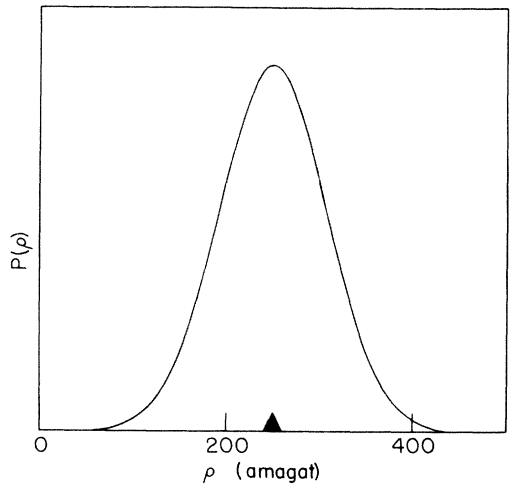

FIG. 13 The probability distribution for local density as determined via Eq. (10) of the text with $\bar{\rho}=\rho_c$ (triangular marker) and $\epsilon=8\times10^{-5}$. The curve is a Gaussian with a full width at half maximum of 140 amagat or $0.55\rho_c$.

The fit of Fig. 12 was considered quite acceptable given that only one adjustable parameter (σ) was involved. However, the fact that the most obvious discrepancies occurred on the high-ν or low-ρ side of the profile(s) suggested some possibilities for refinement. For example, it was recognized at the outset that the Lorentzian approximation of Eq. (10) did not properly account for the known asymmetry of the normal low-density ($\rho<100$) spectrum.[18,19] As a consequence, the modeling of $\nu_p(\rho)$, and to a lesser extent $\Delta(\rho)$, were also subject to improvement.[3] This was attempted in a number of ways, including the use of the generalized line-shape dependence given in Ref. 19. However, it was decided that the marginal improvement in the resulting fit did not warrant the introduction of the additional adjustable parameters required. Generalization of the Gaussian form for $P(\rho)$, i.e., by introducing higher-order terms[22] in the exponential function [Eq. (12)], was also found to have little effect. The remaining option of revising the basic assumptions (i) and (ii) was considered, but no such action was taken because it was not at all clear what form the revisions should take. In any case, it was doubtful whether the magnitude of the broadening effect, and the overall accuracy of the experimental profiles, actually justified further elaboration of the model.

The results presented here (e.g., Fig. 13) represent the first experimental information pertaining to the probability distribution for local density, or more generally speaking the local order parameter (in this case $\rho-\rho_c$), in a near-critical system. The potential contribution of such information to an improved understanding of critical phenomena has been emphasized in recent theoretical[23,24] and

Monte Carlo[25] studies of size effects in magnetic systems. The latter results[25] reveal several points of favorable qualitative comparison with the present $P(\rho)$ data. However, the point of closest contact with theory is provided by the prediction of Ref. 22 that, for $\epsilon \rightarrow 0$, the width of the probability distribution function (e.g., σ in the present case) should exhibit an exponential approach to a maximum value at T_c. This is consistent with the plot of Fig. 14, which summarizes the results of our analysis for all spectra recorded on the critical isochore. We emphasize, however, that the values of σ obtained are only expected to be reliable for spectra which exhibit a pronounced inhomogeneous broadening near T_c. Consequently, Fig. 14 includes a visual straight-line fit which applies only to the lowest ϵ points. The maximum ($\epsilon=0$) value of σ is essentially the same as that obtained for the two lowest temperature spectra (cf. Fig. 13), namely, 60 amagat. This in turn corresponds to a FWHM value for $P(\rho)$ of 140 amagat, or $0.55\rho_c$.

It is noted in passing that the theoretical result in question[22] is based on a (quartic) non-Gaussian model, which should not be regarded as necessarily conflicting with the present Gaussian approximation for $P(\rho)$. Rather, it most probably indicates a relatively low level of sensitivity in the experiments. An important conclusion of the theory[22] is that the precise details of $P(\rho)$ are crucial in predicting a physically plausible behavior for such gross characteristics as its width. On the other hand, as concluded above, the experiment is not yet capable of discerning such fine details since introduction of the quartic non-Gaussian in the analysis procedures leads to essentially the same result (Fig. 14).

A similar comment applies with respect to the most recent (unpublished) Monte Carlo data for the local magnetization in an Ising model.[26] While there is substantial agreement with Fig. 14, the finer details revealed by the computer simulations are beyond the sensitivity of the present experiment, and pose a challenge for future work.

In brief, the extent and accuracy of the information provided by the present methods is primarily limited by the magnitude of the observed broadening effect (in N_2). Work in progress is therefore concentrating on the identification of other systems for which the critical broadening is more pronounced. Preliminary results[27] for H_2 indeed indicate a broadening which is greater by a factor of ~ 3 compared to N_2. These results are, however, subject to confirmation and analysis, and will be published at a later date.

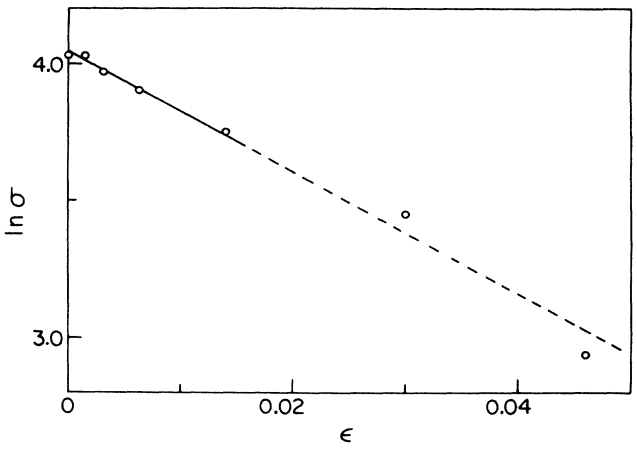

FIG. 14 Natural logarithm of the square root of the $P(\rho)$ second moment σ (in amagat units) versus ϵ on the critical isochore. The solid line is a visual fit, and its dashed extension indicates the region where the method of σ determination is not considered reliable. The linear fit corresponds to $\sigma = 60\exp(-23\epsilon)$.

ACKNOWLEDGMENTS

The authors wish to thank Professor K. Binder for helpful comments and for providing access to unpublished Monte Carlo results. Assistance provided by L. B. Knee and A. P. Smith in computer programming and data analysis is acknowledged. Appreciation is expressed for access to the facilities of the Herzberg Institute of Astrophysics, National Research Council of Canada, during preparation of the manuscript. The work was supported by grants from the Natural Sciences and Engineering Research Council of Canada.

[1]M. J. Clouter and H. Kiefte, J. Chem. Phys. **66**, 1736 (1977).
[2]M. J. Clouter, H. Kiefte, and N. Ali, Phys. Rev. Lett. **40**, 1170 (1978).
[3]M. J. Clouter, H. Kiefte, and R. K. Jain, J. Chem. Phys. **73**, 673 (1980).
[4]M. J. Clouter and H. Kiefte, Phys. Rev. Lett. **52**, 763 (1984).
[5]B. P. Hills and P. A. Madden, Mol. Phys. **37**, 937 (1979).
[6]D. W. Oxtoby, Adv. Chem. Phys. **40**, 1 (1979); W. G. Rothschild, *Dynamics of Molecular Liquids* (Wiley, New York, 1984).
[7]G. Herzberg, *Spectra of Diatomic Molecules* (Van Nostrand, Princeton, 1959).
[8]R. P. Srivastava and H. R. Zaidi, in *Raman Spectroscopy of Gases and Liquids*, edited by A. Weber (Springer-Verlag, New York, 1979).
[9]A. D. May, V. Degen, J. C. Stryland, and H. L. Welsh, Can. J. Phys. **39**, 1769 (1961).
[10]A. D. May and J. D. Poll, Can. J. Phys. **43**, 1836 (1965).
[11]J. O. Hirschfelder, C. F. Curtiss, and R. B. Bird, *Molecular Theory of Gases and Liquids* (Wiley, New York, 1967).
[12]R. K. Jain, M. Sc. thesis, Memorial University of Newfoundland, 1978 (unpublished).
[13]H. L. Strauss and S. Mukamel, J. Chem. Phys. **80**, 6328 (1984).
[14]M. J. Clouter, H. Kiefte, and A. P. Smith, Chem. Phys. Lett. **107**, 83 (1984).
[15]W. May, H. Kiefte, M. J. Clouter, and G. I. Stegeman, Appl. Opt. **17**, 1603 (1978).
[16]E. Hecht and A. Zajac, *Optics* (Addison-Wesley, Reading, 1979).
[17]I. S. Gradshteyn and I. M. Ryzhik, *Table of Integrals, Series, and Products* (Academic, New York, 1965), item 3.613.1.

[18]V. Alekseyev, A. Grasiuk, V. Ragulsky, I. Sobelman, and F. Faizulov, IEEE J. Quantum Electron. **4**, 654 (1968); V. Alekseyev and I. Sobelman, Zh. Eksp. Teor. Fiz. **55**, 1874 (1968) [Sov. Phys.—JETP **28**, 991 (1969)]; S. I. Temkin and A. I. Burshtein, Pis'ma Zh. Eksp. Teor. Fiz. **24**, 99 (1976) [JETP Lett. **24**, 86 (1976)]; Chem. Phys. Lett. **66**, 52 (1979); **66**, 57 (1979); **66**, 62 (1979).

[19]A. D. May, J. C. Stryland, and G. Varghese, Can. J. Phys. **48**, 2331 (1970).

[20]The term amagat denotes the dimensionless relative density ρ/ρ_{STP}, where $\rho_{STP}=0.044\,65$ mole l^{-1} from Ref. 21.

[21]R. T. Jacobsen and R. B. Stewart, J. Phys. Chem. Ref. Data **2**, 757 (1973).

[22]J. A. Tuszyński, M. J. Clouter, and H. Kiefte, Phys. Lett. **108A**, 272 (1985).

[23]M. Thomsen, M. F. Thorpe, T. C. Choy, and D. Sherrington, Phys. Rev. B **30**, 250 (1984).

[24]A. D. Bruce, T. Schneider, and E. Stoll, Phys, Rev. Lett. **43**, 1284 (1979); A. D. Bruce, J. Phys. C **14**, 3667 (1981).

[25]K. Binder, Z. Phys. B **43**, 119 (1981); K. Kaski, K. Binder, and J. D. Gunton, Phys. Rev. B **29**, 3996 (1984); K. Binder and D. P. Landau, *ibid.* **30**, 1477 (1984).

[26]K. Binder (private communication).

[27]M. J. Clouter, H. Kiefte, and C. G. Deacon, Molecular Spectroscopy Symposium, Columbus, Ohio, 1985 (unpublished).